ELSEVIER

Carbohydrate Polymers 50 (2002) 123–132

Carbohydrate Polymers

www.elsevier.com/locate/carbpol

Using AFM to image the internal structure of starch granules

M.J. Ridout, A.P. Gunning, M.L. Parker, R.H. Wilson, V.J. Morris*

Institute of Food Research, Norwich Research Park, Colney, Norwich NR4 7UA, UK

Received 25 January 2001; revised 27 November 2001; accepted 14 December 2001

Abstract

Atomic force microscopy (AFM) has been used to observe the ultra-structure of starch granules for starches from different botanical sources (maize and potato). Starch granules were embedded, sectioned and imaged in dc constant force topographic, error signal and force modulation modes. AFM images of the starches embedded in Nanoplast®, a resin previously used for AFM and electron microscopy studies, failed to reveal the growth ring structure within the granules consistently. Furthermore, ultra-structural features could not unequivocally be attributed to the 'blocklet' structure of the granule because of the underlying granular texture of the resin itself. In contrast the use of rapid setting Araldite, a non-penetrating resin, allowed the ultra-structure of the granules to be viewed without the necessity of pre-treatment (lintnerisation or enzymatic degradation) steps. The images demonstrated clearly the importance of the choice of embedding material, and showed that under the correct conditions 'growth rings' and blocklet structures can be observed in 'near native' granules.

Keywords: Atomic force microscopy; Starch; Optical microscopy; Ultra-structure

1. Introduction

Starch is the major plant storage carbohydrate consumed by mankind. It is an important component of our diet present in starch-rich and processed foods. High-carbohydrate, low-fat diets are promoted as healthy diets, offering protection against certain Western diseases such as colon cancer or heart disease. Starch is synthesised in plants as complex semi-crystalline granules. It is the ultra-structure of the granule that dictates the swelling properties, the release of amylose during gelatinisation and the consequent changes in starch-based products during processing and storage. Thus the structure of the granules ultimately affects the digestion of raw and processed starch-based foods and their fermentation in the colon, and contributes to the protective effects of Resistant Starch. At present, food technologists select different sources of starch for different applications, or chemically modify starches to enhance their functional behaviour. With consumer demands for the reduction of chemical modification, there is considerable scope for exploiting novel physical processing and recent developments in molecular biology, to modify and design starches with desirable structure and properties. Despite the advances in the understanding of starch biochemistry and genetics, there is still incomplete understanding of the bio-assembly of granule structure, and insufficient information on the ultra-structure of granules to allow rational design of starches with desired functional properties. However, there is a growing interest in this field and the current views on granule structure and assembly are covered in a recent review (Buléon, Colonna, Planchot, & Ball, 1998a).

Two classes of starch polysaccharide can be extracted from starch granules: A predominately linear $\alpha(1 \rightarrow 4)$ linked glucan called amylose and a more complex $\alpha(1 \rightarrow 4)$ linked branched glucan called amylopectin. Within the granule, the short branches of the amylopectin are crystalline and determine the level of crystallinity in native starches. Inside the granule the starch polysaccharides are arranged into concentric rings radiating out from the central hilum to the surface of the granule. The number and size of the rings depends on the botanical origin of the starch (French, 1984). The ring structure is enhanced in hydrated (Atkin, Abeeysekera, Cheng, & Robards, 1998), lintnerised (Yamaguchi, Kainuma, & French, 1979) or enzymatically treated granules (Gallant, Mercier, & Guilbot, 1972). Experimental studies suggest that the rings are semi-crystalline and composed chiefly of amylopectin (Buléon, Gérard, Riekel, & Chanzy, 1998b; French, 1984). The exact location of amylose within granules is still being studied and remains unclear (Jane, Xu, Radosavljevic, & Seib, 1992). It has been suggested that rings can be further subdivided into blocklets

* Corresponding author. Tel.: +44-1603-255271; fax: +44-1603-507723.

E-mail address: vic.morris@bbsrc.ac.uk (V.J. Morris).

0144-8617/02/$ - see front matter
PII: S0144-8617(02)00021-8

(Gallant, Bouchet, & Baldwin, 1997) and that, at least in some experiments, these blocklets can be separated from granules during gelatinisation (Atkin et al., 1998). It has been known for some time that the granules exhibit periodical variations in ultra-structure characterized by a 9 nm repeat unit and this feature can be probed by small angle X-ray (SAXS) or neutron (SANS) scattering studies (Jenkins, Cameron, & Donald, 1993; Jenkins & Donald, 1996). Based on scattering data and transmission electron microscopy, various models of the crystalline architecture of starch granules have been proposed (Gallant et al., 1997; Oostergetel & van Bruggem, 1993), including modern suggestions that the helical domains of the amylopectin molecules are arranged in a chiral liquid crystalline structure (Waigh, Perry, Reikel, Gidley, & Donald, 1998).

Scattering methods can be used to follow changes in starch granule structure during gelatinisation (Cameron & Donald, 1992; Jenkins & Donald, 1998; Waigh, Gidley, Komanshek, & Donald, 2000), and have recently been used to propose a two-stage melting process for starch gelatinisation (Jenkins & Donald, 1998). These methods measure average properties for a population of granules and the scattering data is time and spatially averaged. Providing water is not a limiting factor, the heterogeneity of structure within granules plays a very important role in the shape and size changes of the granule during gelatinisation. Little is known about this heterogeneity and microscopy provides the only direct method of probing such structure. Recently, it has been possible to show specific spatial arrangements of different crystal structures within pea granules using synchrotron X-ray microprobe analysis (Buléon et al., 1998a,b) and a novel use of conventional polarised light microscopy, coupled with selective melting of different crystal structures within the granules (Bogracheva, Morris, Ring, & Hedley, 1998). These studies show that there is still much that can be learnt about starch structure, and that innovations in microscopy provide the best route to such discoveries. Currently electron microscopy has been the main tool used to investigate the ultra-structure of starch granules. Small blocklets, of the order of 20–30 nm, have been observed in granules by SEM and TEM (Gallant et al., 1997), and the highest resolution TEM studies revealed stacks of crystalline lamella in lintnerised granules (Yamaguchi et al., 1979). Atomic force microscopy (AFM) studies of granule surfaces have revealed surface protrusions attributed to the ends of blocklets at the surface of the granule (Baldwin, Davies, & Melia, 1997; Baldwin, Adler, Davies, & Melia, 1998; Gallant et al., 1997). Electron microscopy studies often require chemical or enzymatic modification of starch plus embedding, sectioning, evacuation or metal coating of the samples. AFM offers the prospect of examining starch using less stringent preparation conditions, and offers potentially new contrast mechanisms for examining ultra structural models of starch granule architecture. A recent AFM study (Baker, Miles, & Helbert, 2000) employed the embedding and sectioning methods sometimes used in TEM studies of the internal structure of starch granules. In this paper we compare the influence of embedding techniques on the contrast in AFM images of starch, and examine the benefits of other embedding methods for improving resolution of granule structure.

2. Materials and methods

Potato and maize starch were gifts from Dr S.G. Ring at IFR.

2.1. Embedding

Some of the starch samples were embedded in Nanoplast® FB 101 (melamine) resin (Agar Scientific). Before embedding the starch samples were dried in a desiccator over P_2O_5 for 5 days at room temperature. The water-based melamine resin was mixed with the initiator (an acid-based catalyst), the starch granules added, thoroughly mixed and the mixture poured into a mould. This preparation was stored in a desiccator and cured in an oven at 40 °C for 2 days. The sample was removed from the desiccator and heated in the oven at 60 °C for a further 3 days, then cooled to room temperature in a desiccator. The starch occupied about 20% of the volume of the sample.

Some starch was embedded in rapid setting Araldite. This procedure is quicker and simpler. The undried starch was mixed with the rapid set Araldite (Bostik Ltd) then transferred to a mould. The Araldite sets in about 2 min and hardens within 24 h after which time the sections could be cut.

2.2. Sectioning

Sections, nominally 1.5 μm thick, of starch embedded in Nanoplast®, or rapid-setting Araldite were cut onto water with glass knives using an Ultramicrotome (Ultracut E, Reichert-Jung). The sections were immediately transferred to a drop of distilled water on a glass slide. Individual sections were moved from the edge of the drop to an area of dry glass and the slide left to dry at room temperature. Although it was possible to cut thinner or thicker sections, a thickness of 1.5 μm maintained the integrity of the starch granules during sectioning and minimised starch swelling on contact with water.

2.3. Light microscopy

Sections were stained with very dilute iodine in potassium iodide and the starch sections examined and photographed in Olympus BX60 microscope equipped with digital image acquisition software (Syncroscopy).

2.4. Infrared microscopy

Sections in both rapid-setting Araldite and Nanoplast® were studied using a BioRad dynamic alignment FTIR

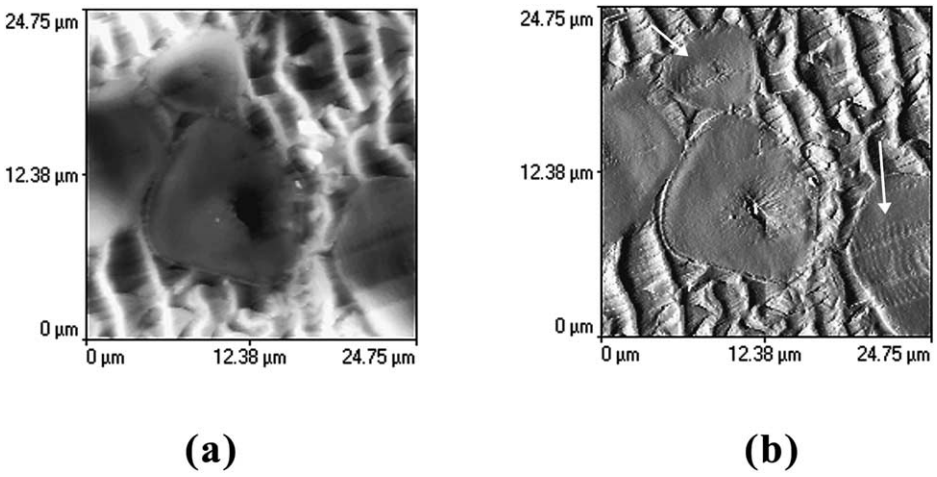

Fig. 1. AFM images of sectioned maize starch granules in Nanoplast® resin: (a) Topography image, (b) error signal image.

Spectrometer FTS 175C to determine penetration of the embedding material. The scanned area was focused down to 8 μm and areas of the resin, resin and granule, and the granule alone were scanned and compared.

2.5. Atomic force microscopy

AFM was undertaken using a Thermomicroscopes Lumina combined AFM/SNOM system. Sections were usually imaged in air using the 'Dry Scanner' attachment. Potato sections under water were scanned using the 'Liquid Scanner' attachment.

In the dc mode of operation the AFM cantilever, on which the tip is mounted, is held at a constant deflection as it traces over features on the sample surface by a feedback loop that controls the operation of the piezoelectric scanner tube. The magnitude of the deflection, and hence the force between tip and sample is determined by the set point of the instrument. 'Topography' images are generated by displaying the changes in the Z direction of the piezoelectric scanner required to restore the deflection of the cantilever to its predefined set point at each image point. Displaying the transient deviations of the cantilever away from the set point as the tip encounters features during scanning generates the 'error signal' image. It effectively represents a differential of the topography image, since it accentuates sharp turning points in the sample topography (high frequency information) at the expense of smooth slowly undulating areas (low frequency information). In the force modulation mode, which is a contact mode of imaging, in addition to the feedback signal required to control the cantilever deflection, a small sinusoidal signal is applied to the Z direction of the piezoelectric scanner thereby modulating the force between sample and tip. Comparing the response of the cantilever to the driving signal quantifies the relative elastic moduli of the sample surface and generates the 'force modulation' image. The grey levels in the image actually represent the gradient of the force versus distance response (elastic modulus) at each sampling point across the sample surface, hence bright regions (high gradient) are comparatively hard and dark regions comparatively soft.

The AFM tip had a nominal spring constant of $0.38\ \mathrm{Nm}^{-1}$. Data collected included topography, error signal and where possible force modulation images.

Scan sizes varied from 100 μm down to 1 μm. The scan rate was generally 2 Hz, except during force modulation measurements when the scan rate was 1 Hz. In force modulation the cantilever was driven at a frequency of 5 kHz into the sample surface with an amplitude of 4.0 nm.

3. Results and discussion

In contrast with many of the previous studies on starch granule sections, in this investigation the starch granules have not been 'treated' prior to or post embedding. In many of the reported studies the starch granules are not only embedded within a resin matrix, but have also been either acid treated (lintnerised) or enzyme treated to enhance many of the internal structural features. (Gallant et al., 1972; Yamaguchi et al., 1979) This approach has been deliberately avoided in order to observe the 'native' granule structure.

The majority of the sectioned starch samples were imaged in air. Fig. 1 shows topography and error signal mode AFM images of sectioned maize starch in Nanoplast®. The topography image (Fig. 1a) shows several granules of a size and shape typical of maize starch. The black hole in the middle of the granule (hilum) is commonly observed in maize starch and represents an air pocket. The striations in the embedding resin are due to knife chatter during sectioning, and are always parallel to the edge of the knife, and probably due to the brittle nature of the resin. More detail is visible in the equivalent error signal mode image (Fig. 1b). The hilum and radial expansion are visible for the central granule and, although there is some evidence for

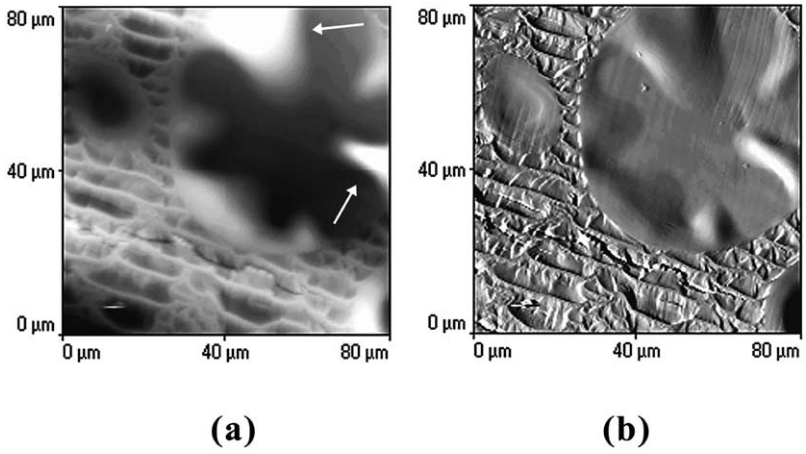

Fig. 2. AFM images of sectioned potato starch granules in Nanoplast® resin: (a) Topography image, (b) error signal image.

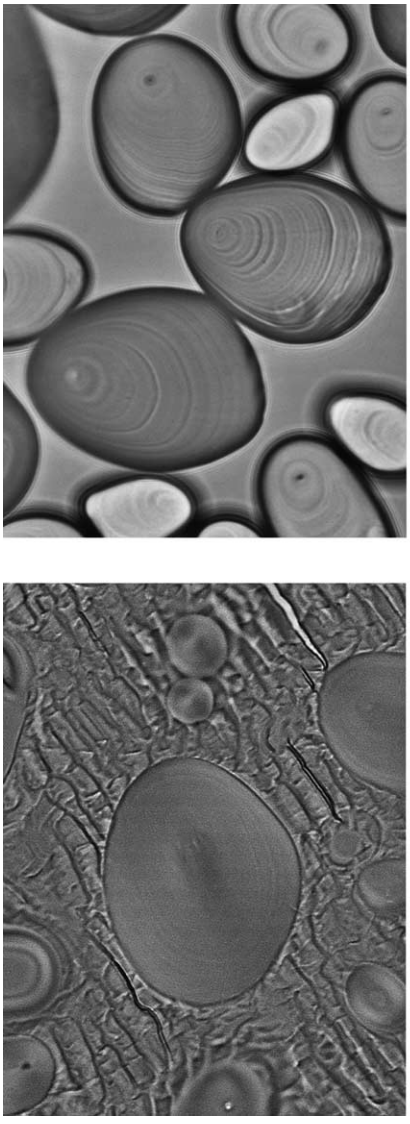

Fig. 3. Optical micrographs of: (a) Whole potato starch granules, and (b) potato starch embedded in Nanoplast® section, both images showing the presence of growth rings.

knife damage on parts (arrowed) of two of the granules, in general the surface of the sectioned granules are smooth and flat. The outer surface of the granules is clearly delineated and this could indicate differences in the nature of this surface or, more likely, results from a change in the motion of the knife at the interface, due to the difference in adhesion at the boundary between the granule and the resin.

Fig. 2 shows equivalent topography and error signal mode AFM images of sectioned potato starch, again in Nanoplast®. In general, images of un-sectioned starch granules (not shown) reveal the presence of populations of both large and small granules observed by light microscopy. Granules of much greater size have been observed, the size range being 25 μm to greater than 120 μm across. Comparison with the light microscopy of whole potato starch granules makes it easier to distinguish between small granules and offset sections of large granules. On the larger granule in Fig. 2a there are a number of folds (arrowed) on the surface of the sectioned granule. These artefacts occur when the section is cut onto water during the sectioning procedure (Gallant & Guilbot, 1971) The starch swells in contact with the water and then forms folds when the section is subsequently dried. The folds seem more marked in the large granules. Again, because of the surface roughness, the error signal mode images reveal more detail (Fig. 2b) and evidence of knife damage can be seen on the surface of some of the sectioned granules.

A general observation is that growth rings are not visible in these AFM images. On a few occasions on parts of some granules there is evidence for growth rings. Growth rings are visible by light microscopy images in whole potato starch (Fig. 3a) and sectioned potato starch in Nanoplast® resin (Fig. 3b), although less obvious in the sections. It is possible that the rings are present, but not observed by AFM because the variation in the contrast is too small.

The AFM is able to resolve surface detail at a higher resolution than the optical microscope. Fig. 4a, b shows topography and error signal mode images of sectioned potato starch granules. The surface of the sectioned granule

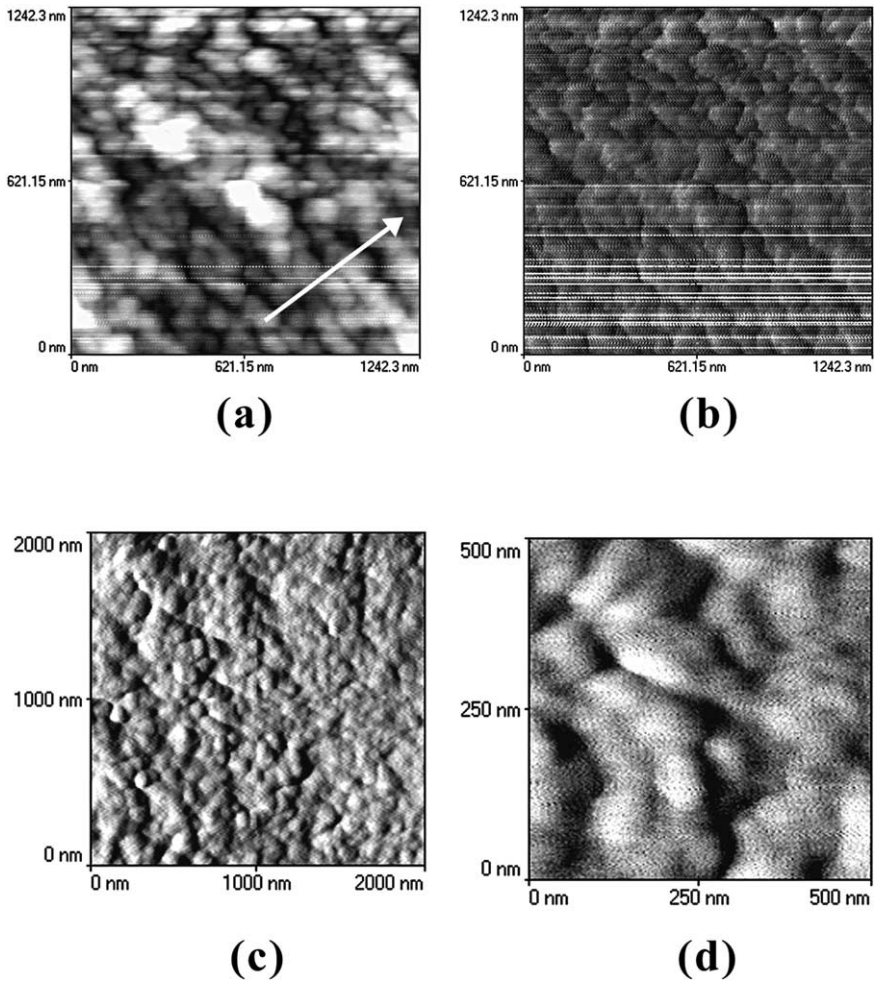

Fig. 4. AFM images of sectioned potato and maize starch granules in Nanoplast® at high magnification. (a) and (b) potato, (c) and (d) maize. (a) Topography, (b, c, d) error signal images.

has a textured appearance with spheroidal objects typically 50–80 nm in size. The radial direction is indicated by the arrow in the topographical image (Fig. 4a). Similar structures are also observed for sectioned maize granules (Fig. 4c, d) for which only error signal mode images are shown. For the maize granules the spheroids are again about 50–80 nm in size. Thus, although growth rings are not readily observable, the high resolution AFM images of sectioned potato and maize starch, embedded in Nanoplast® resin and imaged in air, appear to reveal 'blocklet' structures similar in size and shape to those reported in previous TEM (Gallant et al., 1997) and AFM studies (Baker et al., 2000).

In the AFM the contrast is due to differences in topography on the surface of the sample and/or differences in the elastic modulus of different parts of the section. The folds observed on the surface of the potato starch sections are well-known artefacts of swelling of the starch in contact with water. By imaging under water it may be possible to exploit this swelling behaviour of the sections to improve the contrast in the images. Based on the models for gelatinisation it might be expected that amorphous and crystalline regions within the granule would initially take up water to different extents. The granule should 'bow out' from the section, emphasising differences in topography and modulus between amorphous and crystalline regions of the granule. As the potato starch showed the most evidence for swelling in water these studies were made on sectioned potato starch granules. Fig. 5 shows topography (Fig. 5a), error signal mode (Fig. 5b) and force modulation (Fig. 5c) images of potato starch. Under water, much more detail is seen in the images. Even in the topography and error signal mode images there is evidence for growth rings (arrowed) and substructure within the growth rings. In the force modulation images the growth rings are clearly visible. In true force modulation images the difference in contrast arises solely due to the difference in modulus of the surface. However, in practice, except on very flat surfaces the topography can influence the apparent contrast in the force modulation image. Thus it is only possible to say that the improved contrast in the force modulation image probably results from an enhanced difference in modulus between and within the growth rings. At higher resolution (Fig. 6) the

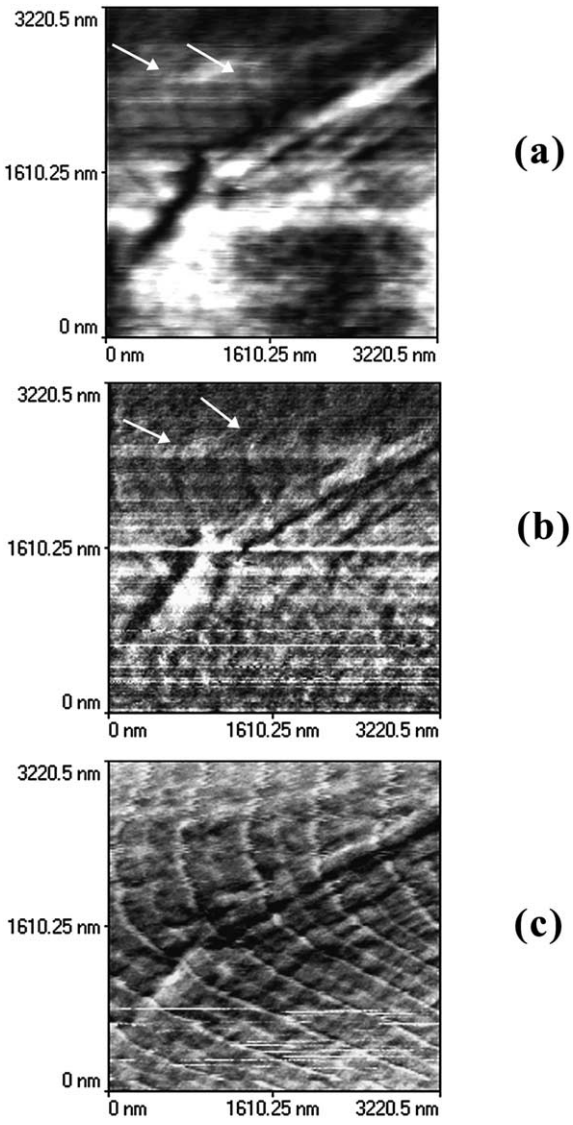

Fig. 5. AFM images of sectioned potato starch in Nanoplast® imaged under water: (a) Topography image, (b) error signal image and (c) force modulation image.

substructure within the rings is more clearly seen in the error signal mode (Fig. 6a) and force modulation (Fig. 6b) images. The contrast is better in the force modulation image. For these smaller scans the surface is flatter, and the differences in contrast in the force modulation images are more likely to reflect differences in modulus, with the brighter regions representing stiffer (crystalline) structures.

The data shown to date, collected on sectioned starch, prepared based on methods used previously for TEM and AFM studies, seems to reveal similar substructures within the granules. It is interesting to consider why it is difficult to visualise the growth rings by AFM. The contrast mechanisms in AFM are different to those for TEM and light microscopy. In the AFM the contrast will be due to sample topography but will also be influenced by differences in sample elasticity. Differences in modulus within the section will be the sole origin of contrast in true force modulation images of flat surfaces, but differences in modulus will also lead to differences in contrast in topography and error signal mode images. Therefore, for AFM imaging of embedded, sectioned samples it is particularly important to consider the effect of the potential penetration of resins into the sample on the AFM images.

Fig. 7 shows Infrared Spectra recorded in an infrared microscope for the resin alone and the region within the starch granules. Nanoplast® resin shows characteristic IR peaks (arrowed) at 1580, 1380 and 810 nm^{-1}. The spectra in Fig. 7a show that characteristic peaks for the Nanoplast® resin are observed within the starch granules indicating that the resin has penetrated the granules. If the resin completely penetrates the granule then it is possible that the modulus of the resin may predominate and obscure small local differences in modulus due, for example, to the growth ring structure. Clearly there is a difference in modulus between the resin background and the granule because the granules are visible in the section, but the differences due to the growth rings may be masked and only visible under water when the differences are enhanced. If the modulus of the resin influences the contrast in the image then it is necessary to show

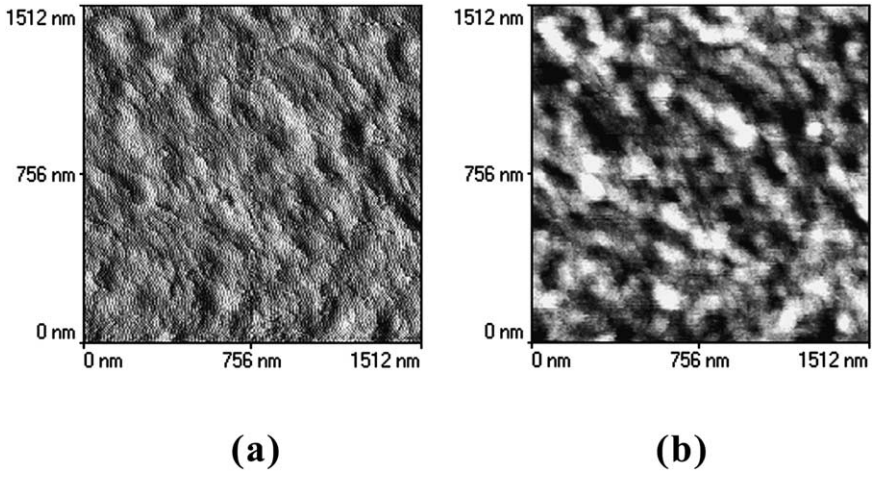

Fig. 6. AFM images of sectioned potato in Nanoplast® imaged under water at high magnification: (a) Error signal image. Note the noise in this image is due to gain ripple, (b) force modulation image.

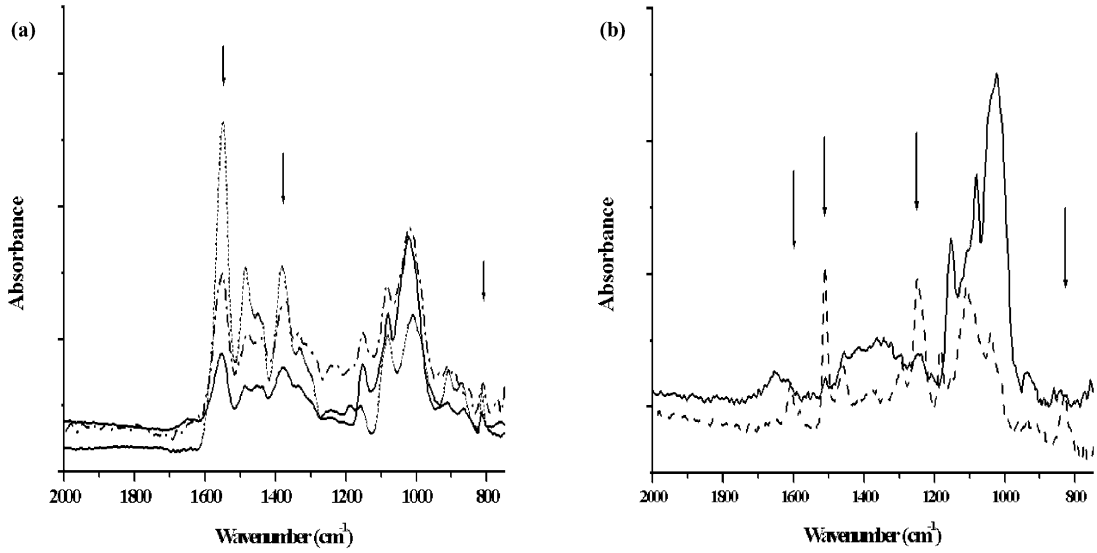

Fig. 7. Fourier Transform Infra Red Spectra of starch granule sections: (a) Nanoplast®, (b) Araldite: (—) Potato starch, (– – –) Resin, (–·–·) Maize starch.

that the resin structure does not interfere with the structure seen in the high-resolution images. Fig. 8a shows an error signal image at high resolution on the Nanoplast® resin. It can be seen that the resin itself exhibits a granular appearance that could be confused with any 'genuine' blocklet structures within starch granules. This 'granular' structure has a size range of 60–110 nm, which covers the range attributed to the blocklet structure of both the potato and maize samples in this study. It may be possible to discriminate between the size of the granular structures seen on the resin alone, and within starch granules. However, the structure of the resin will depend on the local concentration, which will depend on how readily the resin diffuses into different granules. Hence it is difficult to unambiguously attribute granular features, seen for starch embedded in Nanoplast®, to the granule itself or to the resin. Embedding the granules in a non-penetrating resin that shows no granular appearance at high resolution could eliminate this difficulty. In the current study it has been found that a rapid setting Araldite resin fulfils these conditions.

Fig. 7b shows the Infrared spectral data for the rapid-set Araldite alone and the sectioned starch granules. The characteristic peaks (arrowed) for the resin at 1610, 1500, 1260 and 840 nm^{-1} are absent for spectra collected within the boundaries of the granules indicating that the resin has not penetrated the granules. Fig. 8b shows an error signal mode image of the rapid-set Araldite resin showing that the resin surface is featureless (except for gain ripple) at the higher resolution obtained by AFM. Thus, features observed in images within sectioned starch granules should be representative of granule structure.

The light microscopic images of sectioned starches stained with dilute iodine in potassium iodide show interesting differences for the two resins (Fig. 9), which can be attributed to the embedding process. The starch granules embedded in Nanoplast® stain brown whereas, those

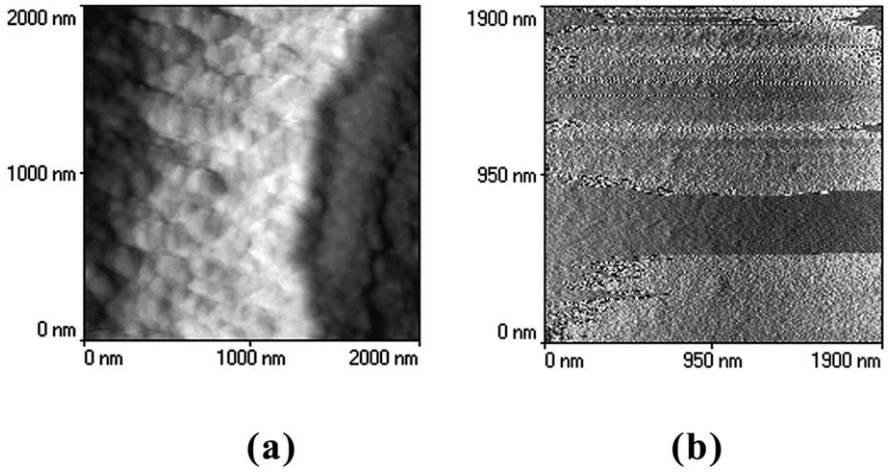

Fig. 8. AFM images of the sectioned embedding resin: (a) Nanoplast®, (b) Araldite.

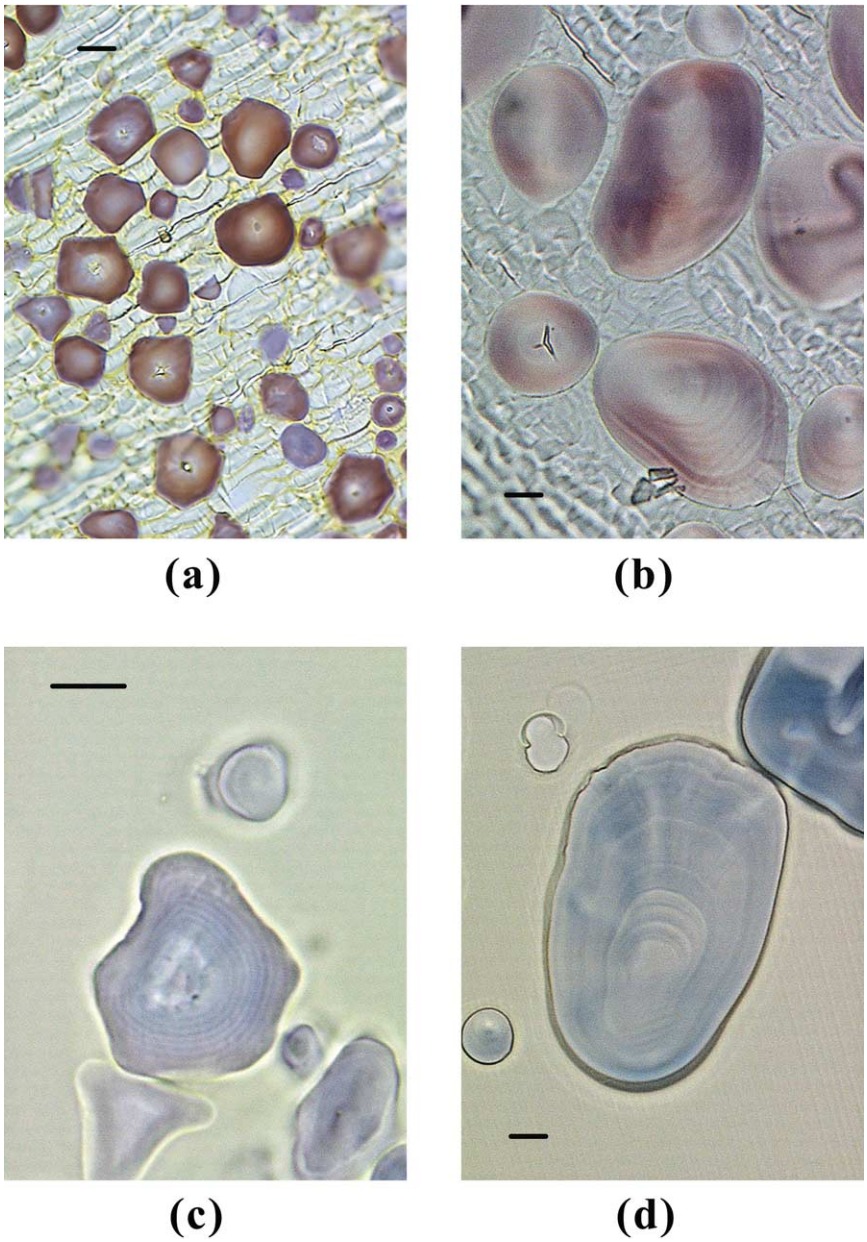

Fig. 9. Optical microscopy of granules stained with dilute iodine in potassium iodide in Nanoplast® (a, b) and rapid-set Araldite (c, d). (a and c) Maize starch, (b and d) Potato starch. Bar represents 10 μm.

embedded in Araldite stain blue. It is generally assumed that amylose stains blue. However, the colour of the complex changes with the degree of polymerisation of the amylosic chains, with shorter chains staining red, brown or yellow. The most straightforward explanation for the brown staining for starch embedded in Nanoplast® is that the amylose has been at least partially degraded. Nanoplast® contains 70% hexa- methylol-melamine methyl ether and *p*-toluene sulphonic acid. The *p*-toluene sulphonic acid is a strong acid and, under the preparation and curing conditions used in the present studies, it is possible that the starch is partially lintnerised. If the amylose degrades and recrystallises during embedding in Nanoplast® then this could introduce artefacts into the images observed by both TEM and AFM. This provides further impetus for the use of a non-penetrating resin for embedding the starch. In addition the ring structure is clearly seen in the sections embedded in rapid-set Araldite.

Fig. 10 shows AFM images of sectioned maize starch embedded in rapidly setting Araldite, imaged in air. The topography image (Fig. 10a) shows a central hole and radial cracks but little fine detail of granule structure. However, in the error signal mode (Fig. 10b) and force modulation images (Fig. 10c) the growth ring structure is clearly visible, in contrast to the data presented for maize in Nanoplast®. The growth rings are better defined in the force modulation

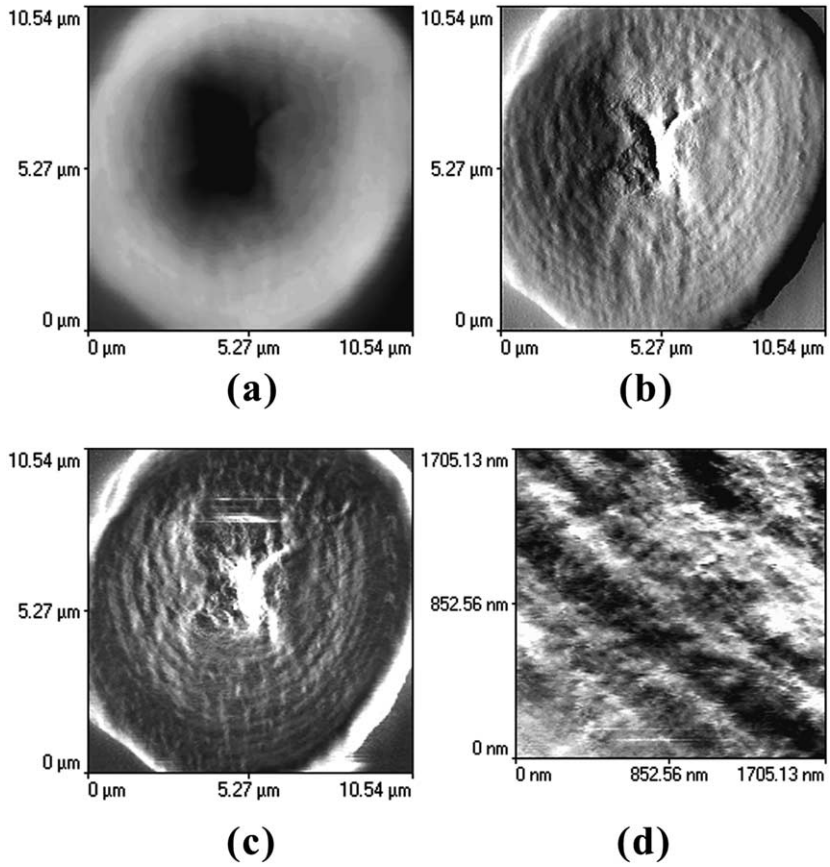

Fig. 10. AFM images of sectioned maize starch granule in rapid-set Araldite: (a) Topography image, (b) error signal image, (c) force modulation image and (d) high magnification force modulation image.

image where in this case, it is likely that the topography image is enhanced by differences in modulus, rather than being entirely determined by such differences. At higher resolution the force modulation (Fig. 10d) images show evidence for globular structures within, and across the growth rings. These globular features range from 45 to 85 nm in size and are unambiguously true features of the starch granule structure. Interestingly, in the cases described here there is little evidence to suggest that there is a difference in size of the blocklets across or within the growth rings. The contrast mechanism used by AFM indicates that the blocklet size is constant across the exposed surface, on the contrary to the model proposed recently (Gallant et al., 1997).

4. Conclusions

It is possible to image starch granule structure by AFM after embedding and sectioning. Despite the flatness of the sample, differences in elastic modulus across the sample are believed to enhance contrast in the images. The nature of the embedding resin used affects the images obtained. An interpenetrating resin such as Nanoplast® appears to reduce contrast, inhibiting the ability to observe features such as growth rings, and may introduce globular features that would make it difficult to image unambiguously the expected blocklet structure of the granule. Iodine in potassium iodide staining of embedded sections suggests that under certain preparative conditions, embedding in Nanoplast® may alter the structure within the starch granules, introducing artefactual structures observable by TEM or AFM. Use of a non-penetrating resin such as rapid-setting Araldite overcomes these difficulties. Better contrast is obtained thus allowing growth rings and ultra-structure to be observed in unstained, untreated granules: The granules do not need to be lintnerised or modified by enzymes in order to reveal growth rings. Force modulation images show improved contrast, when compared to error signal mode imaging. This suggests that differences in elastic modulus within the starch granule contribute to contrast in the images, and that the AFM images should be sensitive to the location of amorphous and crystalline regions within the granules. Features probably attributable to blocklets appear as higher contrast presumably stiffer, higher modulus units, consistent with a partially crystalline structure. The AFM provides novel contrast mechanisms and AFM images will complement SEM and TEM data. The data shown in Fig. 10 are probably the first images of the ultra-structure in native, unstained and unmodified starch granules. The methodology

could be used to compare starches from different botanical sources or to examine the effects of genetic mutations on starch granule structure. It may also be possible to adapt the procedures to follow changes in starch granule structure during gelatinisation or retrogradation on storage.

Acknowledgements

This research was supported by the BBSRC through the core grant to the Institute and through the award of a Bioimaging Grant, D11154, allowing the purchase of the combined AFM/SNOM microscope.

References

Atkin, N. J., Abeeysekera, R. M., Cheng, S. L., & Robards, A. W. (1998). An experimentally based predictive model for the separation of amylopectin subunits during starch gelatinisation. *Carbohydrate Polymers*, *36*, 173–192.

Baldwin, P. M., Davies, M. C., & Melia, C. D. (1997). Starch granule structure imaging using low-voltage scanning electron microscopy and atomic force microscopy. *International Journal of Biological Macromolecules*, *21*, 103–107.

Baldwin, P. M., Adler, A. J., Davies, M. C., & Melia, C. D. (1998). High resolution imaging of starch surface granules by atomic force microscopy. *Journal of Cereal Science*, *27*, 255–265.

Baker, A. A., Miles, M. J., & Helbert, W. (2000). Internal structure of the starch granule revealed by AFM. *Carbohydrate Research*, *330*, 249–256.

Bogracheva, T. Ya., Morris, V. J., Ring, S. G., & Hedley, C. L. (1998). The granular structure of C-type pea starch and its role in gelatinisation. *Biopolymers*, *45*, 323–332.

Buléon, A., Colonna, P., Planchot, V., & Ball, S. (1998a). Starch granules: Structure and biosynthesis. *International Journal of Biological Macromolecules*, *23*, 85–112.

Buléon, A., Gérard, C., Riekel, C., Vuong, R., & Chanzy, H. (1998b). Details of the crystalline ultra-structure of C-starch granules revealed by synchrotron microfocus mapping. *Macromolecules*, *31*, 6605–6610.

Cameron, R. E., & Donald, A. M. (1992). A small angle X-ray scattering study of the annealing and gelatinisation of starch. *Polymer*, *33*, 2628–2636.

French, D. (1984). In R. Whistler, E. F. Paschell & J. N. BeMiller, *Starch chemistry and technology* New York: Academic Press.

Gallant, D. J., & Guilbot, A. (1971). Artefacts au cours de la preparation de coupes de grains d'amidon. Etude par microscopie photonique et électronique. *Starch/Stärke*, *23*, 244–250.

Gallant, D., Mercier, C., & Guilbot, A. (1972). Electron microscopy of starch granules modified by bacterial α-amylase. *Cereal Chemistry*, *49*, 354–365.

Gallant, D. J., Bouchet, B., & Baldwin, P. M. (1997). Microscopy of starch: Evidence for a new level of granule organisation. *Carbohydrate Polymers*, *32*, 177–191.

Jane, J., Xu, A., Radosavljevic, M., & Seib, P. A. (1992). Location of amylose in normal starch granules. I. Susceptibility of amylose and amylopectin to cross-linking reagents. *Cereal Chemistry*, *69*, 405–409.

Jenkins, P. J., Cameron, R. E., & Donald, A. M. (1993). A universal feature in the structure of starch granules from different sources. *Starch/Starke*, *45*, 417–420.

Jenkins, P. J., & Donald, A. M. (1996). Application of small angle neutron scattering to the study of the structure of starch granules. *Polymer*, *37*, 5559–5568.

Jenkins, P. J., & Donald, A. M. (1998). Gelatinisation of starch: A combined SAXS/WAXS/DSC and SANS study. *Carbohydrate Research*, *308*, 133–147.

Oostergetel, G. T., & vanBruggem, E. F. J. (1993). The crystalline domains in potato starch granules are arranged in a helical fashion. *Carbohydrate Polymers*, *21*, 7–12.

Waigh, T. A., Perry, P., Reikel, C., Gidley, M. J., & Donald, A. M. (1998). Chiral side-chain liquid-crystalline polymeric properties of starch. *Macromolecules*, *31*, 7980–7984.

Waigh, T. A., Gidley, M. J., Komanshek, B. U., & Donald, A. M. (2000). The phase transformations in starch during gelatinisation: A liquid crystalline approach. *Carbohydrate Research*, *328*, 165–176.

Yamaguchi, M., Kainuma, K., & French, D. (1979). Electron microscopic observations of waxy maize starch. *Journal of Ultrastructure Research*, *69*, 249–261.